16th IMEKO TC10 Conference
"Testing, Diagnostics & Inspection as a comprehensive value chain for Quality & Safety
Berlin, Germany, on September 3-4, 2019

Multiple Heat Source Estimation by using Backward Simulator

Yukio Hiranaka

Yamagata University, Yonezawa, Japan, zioi@yz.yamagata-u.ac.jp

***Abstract* –The exact inverse solutions for real measurements are becoming realistic with the progress of computational performances. As an example, heat generation and release transients can be estimated from the temperature measurement if the thermal model is known. Although the inverse solver needs the correct knowledge of the target model, the method of backward simulation has a capability of determining the model structure and the model parameters by itself. A simple case of one heat source model has been shown as a successful example. In this paper, we describe an application of the method to a two heat source case, and show its result for a simulated temperature data.**

Keywords – Heat Source, Heat Transfer, Inverse Problem, Backward Simulation.

I. INTRODUCTION

For machine diagnostics, it may be effective to know the thermal structure and to identify heat sources inside the machine. It is common practice to estimate heat generation amount, heat source position and heat transfer characteristics from temperature measurements [1,2], including deconvolution and super resolution techniques [3,4]. However, such estimation is difficult if the temperature measuring point is far from the heat source or the number of measuring points is insufficient. Inverse heat transfer estimation is usually an ill-conditioned problem [5,6].

However, inverse calculation methods are becoming practical with the progress of computer performances [5,6]. If the thermal model is known, the heat input can be precisely estimated by inverse solvers with applying the measured temperature data [2].

Also, artificial neural network (ANN) method performing optimum estimation using a large amount of measurement data has become practical [7-14]. Even in the field of heat transfer problem, there exist a method to estimate the amount of heat generation from temperature change [12], a method to estimate the amount of heat generation from temperature distribution [13], a method to estimate heat source position from temperature distribution [14]. Mostly, those ANN methods estimates a few number of values such as heat generation in Watt by assuming the thermal structure.

The authors have been conducting researches by using the backward simulation technique [15-17] to estimate the time change of heat generation from the temperature change at one point in the experiment room. The method supposes the heat conduction model as a simple model and uses one shot measurement data without requiring a large amount of data for learning like ANN.

The backward simulation, one of inverse solvers, estimates heat generation in time sequence based on the energy conservation law and the proportionality of heat transfer to the amount of heat [15-17]. It was shown that the heat transfer coefficients between energy storage elements can also be determined by backward simulation, so that the heat generation can be estimated even if the model structure is not exactly known [17]. Of course, the certainty and the adaptability of the thermal model are important. As the heat phenomenon can be simplified by heat capacities with proportional heat transfers, they can be basically satisfied.

In practical applications, we have to deal the cases of heat generation at one point and heat leakage at another point or surroundings. In such cases, we have to install multiple temperature sensors to estimate both of the time changes of heat sources, positive or negative. This paper describes a method and results for such estimation by using transient temperature changes at two measuring points.

II. BACKWARD SIMULATION

Fig.1 shows a room which has a heat source (the human in the figure), local heat accumulation by air mass, and heat leak through the wall. The temperature changes (y_2, y_3) are measured in two places in order to calculate the two heat sources inside and outside. To match the situation, our model consists of four heat storage nodes corresponding to the air mass surrounding the heat source (u_1), its vicinity's air mass u_2 (the first temperature measuring point), the whole room air mass u_3 (the second temperature measuring point), the wall u_4, and heat sources of the inside generator x_1 and the heat source x_4 which corresponds to the outflowing negative heat source.

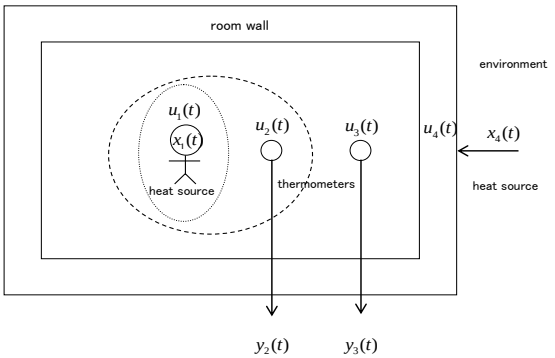

Fig. 1. Inverse problem of heat transfer estimation.

Fig. 2 shows a simplified model of heat storages of heat capacities C_1, C_2, C_3 and C_4. The transfer coefficients between them are k_{12}, k_{21}, k_{23}, k_{32}, k_{34} and k_{43}. Assuming that the heat transfer between the heat storages is proportional to the amount of heat, the following equations in relation to time t and t + 1 holds,

$$u_1(t+1) = (1-k_{12})u_1(t) + x_1(t) - k_{21}u_2(t), \quad (1)$$

$$u_2(t+1) = (1-k_{21}-k_{23})u_2(t) + k_{12}u_1(t) + k_{32}u_3(t), \quad (2)$$

$$u_3(t+1) = (1-k_{32}-k_{34})u_3(t) + k_{23}u_2(t) + k_{43}u_4(t), \quad (3)$$

$$u_4(t+1) = (1-k_{43})u_4(t) + x_4(t) + k_{34}u_3(t), \quad (4)$$

$$y_2(t) = u_2(t)/C_2, \quad (5)$$

$$y_3(t) = u_3(t)/C_3. \quad (6)$$

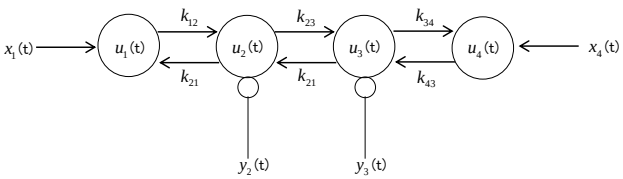

Fig.2. Four heat storage model.

Our objective is to obtain $x_1(t)$ and $x_4(t)$ by calculating $u_1(t)$, $u_2(t)$, $u_3(t)$ and $u_4(t)$ from the measured temperatures $y_2(t)$ and $y_3(t)$. The heat amounts $u_2(t)$ and $u_3(t)$ are directly known from $y_2(t)$ and $y_3(t)$. The remaining values of $u_1(t)$, $u_4(t)$, $x_1(t)$, $x_4(t)$ are calculated as follows,

$$u_1(t) = \frac{u_2(t+1) - (1-k_{21}-k_{23})u_2(t) - k_{32}u_3(t)}{k_{12}}, \quad (7)$$

$$u_4(t) = \frac{u_3(t+1) - (1-k_{32}-k_{34})u_3(t) - k_{23}u_2(t)}{k_{43}}, \quad (8)$$

$$x_1(t) = u_1(t+1) - (1-k_{12})u_1(t) - k_{21}u_2(t), \quad (9)$$

$$x_4(t) = u_4(t+1) - (1-k_{43})u_4(t) - k_{34}u_3(t). \quad (10)$$

It is a backward calculation in which the values in the previous time are obtained from the data of the later time. In the cases that we do not know the exact values of heat transfer coefficients, we have to determine them by searching the condition conforming physical laws. As the conformity used for the judgment, we used the fact that any heat values must be nonnegative. If the heat amount of each storage $u_1(t)$, $u_2(t)$, $u_3(t)$ and $u_4(t)$ or heat generation $x_1(t)$ becomes negative through the calculation, it indicates that the simulated combination of parameters is not feasible.

Heat flow between nodes in the backward calculation can be easily determined because it can be performed by one-way calculation as shown in Fig. 3 unlike the case of one heat source described in [8]. The broken line in the figure represents the link transmitting heat contrary to the flow of the actual heat. The solid line represents the link where the reverse flow can be processed with the forward flow in the equation (7)-(10). Although there are six heat transfer coefficients, they have the following relationship with the ratios of heat capacities. Then, the three transfer coefficients can be determined by other parameters,

$$\begin{aligned} k_{21} &= k_{12}C_1/C_2, \\ k_{32} &= k_{23}C_2/C_3, \\ k_{43} &= k_{34}C_3/C_4. \end{aligned} \quad (11)$$

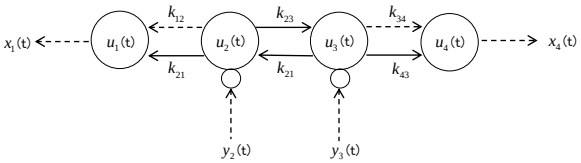

Fig. 3. Backward heat simulation model.

III. SIMULATOR IMPLLEMENTATION

Our simulator was implemented by using Node-RED [18] (Fig. 4). The coefficients of the backward calculation formula, the heat amount in each storage, the heat transfer, and the temperature values are all processed as range signals [15]. There is no concern of the simulation case leakage which is unavoidable by discrete simulations. The ranges of the signals are determined by dividing all possible range by the parameter ndiv. For example, in the case that k_{12} can be any value between 0 to 1 and if we set ndiv as 100, the range for k_{12} is tried from 0 to 0.01, 0.01 to 0.02, and so on.

Since increasing the ndiv takes calculation time proportional to $ndiv^2$ for the simulation, we adopted a reducing method which doubles ndiv stepwise. The range that is shown not feasible in the previous step is not calculated in the subsequent steps by using an array of conformance results. To allow some errors in calculation

for testing non-negative condition, the error allowance is introduced.

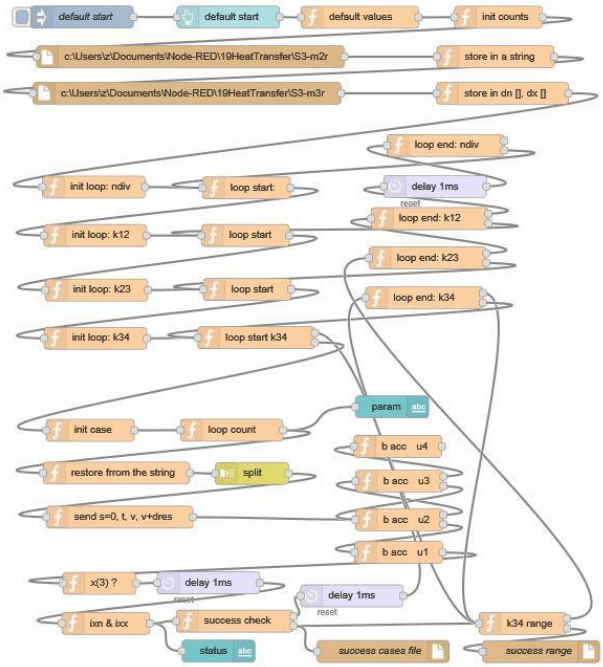

Fig.4. Backward simulation program using node-red.

IV. TEST DATA AND ITS RESULT

The time sequence of x_1 (1 only at t = 6-9, otherwise 0) and x_4 (-0.01 only at t = 21-60, otherwise 0) is shown in Fig. 5. The temperature y_2 and y_3 were determined by equations (1)-(6). The result obtained by setting $k_{12} = 0.3$, $k_{23} = 0.1$, $k_{34} = 0.05$, $C_1 = 1$, $C_2 = 4$, $C_3 = 8$ and $C_4 = 40$ is shown in Fig.6.

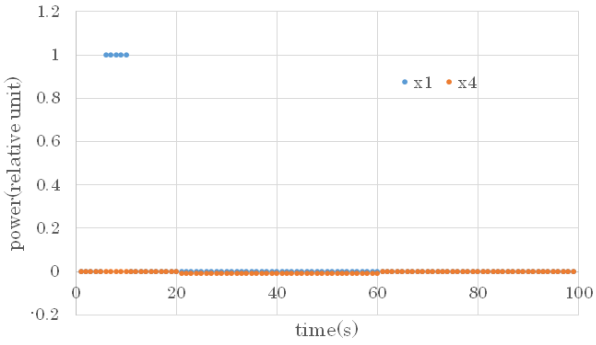

Fig.5. Simulated heat input(x1 and x_2).

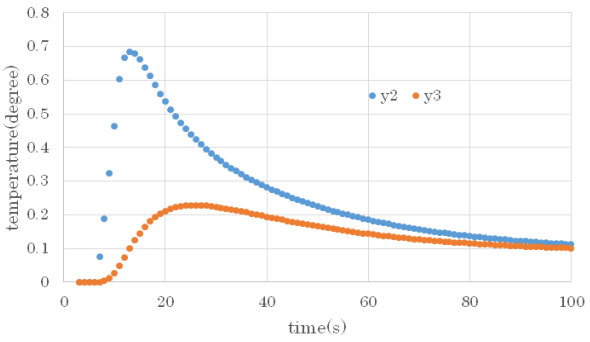

Fig.6. Simulated temperature change (y_2 and y_3).

To confirm that the reverse calculation can be correctly performed, the backward calculation was performed for the correct set of k_{12}, k_{23}, k_{34}, C_1, C_2, C_3 and C_4, and shown in Fg7 and Fg8. The result of x_4 is perfect, while the result of x_1 has some distortion. The larger the value such as k_{12}, the larger the distortion.

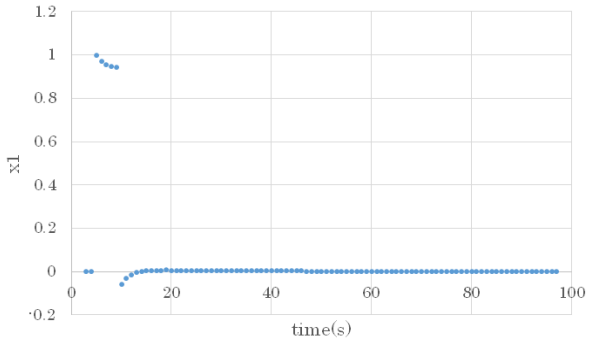

Fig.7. Estimated heat input x_1.

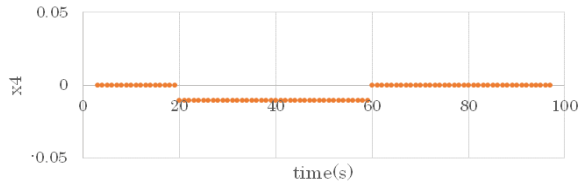

Fig.8. Estimated heat input x_4.

In our simulations, parameters such as k_{12} are searched assuming that C_1, C_2, C_3 and C_4 are known. The entire range is divided into ndiv divisions for k_{12}, k_{23} and k_{34}, and it is mapped whether the conforming data is obtained or not for each combination of parameters. The result maps are shown in Fig. 9 (k_{12} vs. k_{23}) and Fig. 10 (k_{23} vs. k_{34}). The central upper left edge in Fig. 9 indicates the correct value of k_{12}, and the lower right corner in Fig. 10 indicates the correct values of k_{23} and k_{34}.

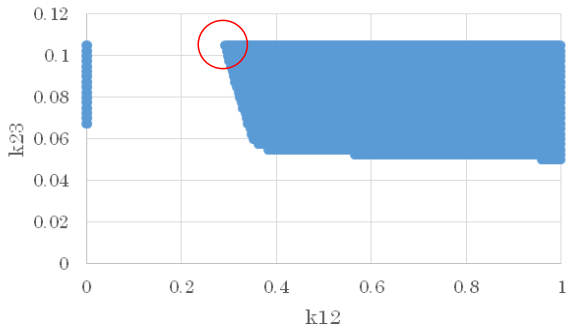

Fig.9. Feasible parameter map for ndiv=400.

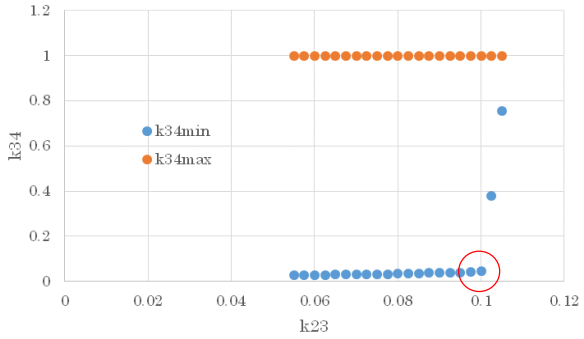

Fig.10. Feasible parameter map for ndiv=400 and k_{12}=0.5.

The reason why k_{12}, k_{23} and k_{34} can be determined from Fig. 8 and Fig. 9 is as follows. At first, the descending part after the peak of y_3 curve in Fig. 6 does not fall more rapidly than that. For example, if x_1 has additional heat input at a time later than the simulation setting, the temperature at each point in the transfer route will rise, but the fall after that will be limited by the outflow parameter k_{34}. On the other hand, even if the descending rate is high, the descent can be changed arbitrarily slow by adding the x_1 input during the descent. Therefore, the descending rate appearing in the graph at times when there is no x_1 input will mainly represent the minimum value of k_{34}. Similarly, the descent part after the peak of y_2 curve in Fig. 6 represents the minimum value of k_{23}.

If k_{34} is tried for all values in the possible range between 0.0 and 1.0, allowing any possible time change of x_1, the feasible value of k_{34} fitted to the curve must be equal to or more than the value corresponding to the descending rate represented by the y_3 curve. Of course, we have to run simulations with sufficient accuracy. However, the values of k_{23} and k_{43} also affect the descent of y_3. Since k_{43} is determined by k_{34} as in the equation (11), only k_{23} must be considered. If k_{23} increases, which means inflow increase to u_3, the outflow parameter k_{34} must be increased to match the increase to keep the descent rate of y_3 unchanged. Therefore, if a value that fits the temperature measurement curve in two dimensions of parameters k_{23} and k_{34} is obtained as shown in Fig. 10, k_{34} will be close to the correct value (0.05) when k_{23} is small. When k_{23} is lager then some value, feasible k_{23} will go up and the corner of the feasible range appear in the lower right of the figure. This corner corresponds the point where the range of feasible k_{34} is unduly reduced by k_{23} value, which means k_{23} beyond the corner is not valid.

On the other hand, the rising of the graph y_2 in Fig. 6 mainly depends on k_{12}, which determines the inflow to u_2. The rise can be made steeper by arbitrarily setting of x_1 input, but the slowest rise with no x_1 input is determined by k_{12}. For the same reason as k_{34}, the minimum value of the curve matching k_{12} will represent the actual value of k_{12}. Since the rise of y_2 also becomes slow as the outflow coefficient k_{23} becomes large, the range of k_{12} and k_{23} that fit in the two dimensional map is determined as shown in Fig. 9. The corner at the upper center represents the minimum value of k_{12} in the feasible range of k_{23}. Then, the actual value of k_{12} can be determined as 0.3 (correct value). Also at the corner, k_{23} is 0.1 and we find that it is appropriate to estimate k_{34} at the lower right corner of Fig.10.

In the application to real measurements, the heat capacities C_1, C_2, C_3, and C_4 have to be determined by the simulation, it is necessary to comprehensively test the conformity for the capacities other than the transfer coefficients. It needs further reduction of calculation time to perform such simulations.

Although the simulation tool Node-RED is a convenient simulation tool, it takes long computation time because of interpreting JavaScript language. It took about 30 minutes for calculation of ndiv = 100 in the case of 100 measured data points. However, the processing time can be largely reduced by concentrating only in the boundary of the conforming area in the Fig. 9 and Fig. 10, more specifically concentrating only in the effective area for parameter determination.

V. REAL MEASUREMENT DATA AND ISSUES

Fig. 11 shows the results of transient temperature change caused by an infrared heater (800W) activated for three minutes and measured by two temperature sensors in a small room. The sensors were placed at two locations in the room (near and far from the heater). Because of some issues we are still in the way to estimate the model parameters k_{12}, k_{23} and k_{34}.

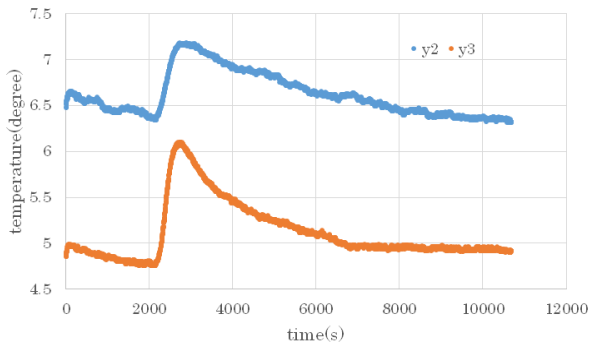

Fig.11 An example of a real temperature change.

There are noise and continuous temperature drift, which is clearly shown before the rising of temperature changes. It is expected that the drift is a contribution of negative heat source corresponding to the external environment and can be used to estimate the negative heat value.

The influence of noise should be suppressed to get a precise estimation. First, with regard to the quantization noise, we convert the measured values to value ranges, of which range width is half the quantization step. With regard to the noise above the quantization step, there is a method of correcting the value of each time point by checking the model match described in [16]. However the calculation time tend to be huge, we are considering to use optimal search method such as used in ANN processings.

Furthermore, the heat capacity ratios C_1/C_2, C_2/C_3, and C_3/C_4 are supposed to be known in the previous sections. However, for practical applications, it is necessary to treat them as unknown. Also, the range of these ratios may not be limited. Therefore, we should search the six parameters of k_{12}, k_{21}, k_{23}, k_{32}, k_{34} and k_{43} all in the range of 0 to 1, basically exhaustively. Since it is a six-dimensional grid search, the calculation time will be huge again. As a little relief, one of the six dimensions can be searched at only the end points of feasible ranges, so that the search is substantially five-dimensional. As an example in the case of k_{34}, Fig. 10 shows that our task is to find only the minimum and the maximum of feasible k_{34} values. To handle five-dimensional search area, we are doubling the parameter ndiv stepwise to get more precise results. In the course, if we find nonconformity to the model in some search area, we can omit the area in the further search. Currently, it takes several days for calculation in the case of ndiv 32 for 200 time point measurement data. We are looking for further time savings.

VI. CONCLUSIONS AND OUTLOOK

It was shown that the time-series estimation of internal conditions and external factors by backward simulation can be effectively done for multiple measured time series. If the number of model parameters to be determined increases, the processing time will be extended. However, we can shorten the processing time by using high performance algorithm and hardwares, and we expect to apply the method effectively to real measured data.

REFERENCES

[1] **J. V. Beck, B. Blackwell and C.R.S. Clair Jr**., Inverse Heat Conduction Ill-posed Problems, John Wiley & Sons, 1985, ISBN 0-471-08319-4.

[2] **Y. Jarny and D. Maillet**, Linear Inverse Heat Conduction Problem – Two Basic Examples, http://www.sft.asso.fr/Local/sft/dir/user-3775/documents/actes/Metti5_School/Lectures%26Tutorials-Texts/Text-L10-Jarny.pdf.

[3] **T.B.Bako and T.Daboczi**, Improved-Speed Parameter Tuning of Deconvolution Algorithm, IEEE Trans. Instrum. Meas., vol.65, no.1, pp.1568-1576, 2016.

[4] **A.Muqaibal, A,Safaai-Jazi, B.Woerner and S.Raid**, UWB Channel Impulse Response Characterization Using Deconvolution Techniques, Proc. MWSCAS, 2002.

[5] **Kenji Oguni**, Inverse problem and instrumentation, Ohmsha, Tokyo, 2011, ISBN 978-4-274-06829-4.

[6] **C.D. Twigg and D.L. James**, Back Steps in Rigid Body Simulation, ACM trans. Graph., vol. 27, no.3, article 25, 2008.

[7] **Ibrahim Mohamed Elshafiey**, Neural network approach for solving inverse problems, https://lib.dr.iastate.edu/rtd/16966, 1991.

[8] **Housen Li, Johannes Schwab, Stephan Antholzer, Markus Haltmeier**, NETT: Solving Inverse Problems with Deep Neural Networks, arXiv preprint arXiv:1803.00092, 2018.

[9] **Liqiang Zhang, Luoxing Li and HuiJu BiwuZhu**, Inverse identification of interfacial heat transfer coefficient between the casting and metal mold using neural network, Energy Conversion and Management, vol. 51, Issue 10, pp.1898-1904, 2010.

[10] **S. Deng and Y. Hwang**, Applying neural networks to the solution of forward, and inverse heat conduction problems, International Journal of Heat and Mass Transfer, 49, pp. 4732–4750, 2006.

[11] **M. Heidari and M. Garshasbi,** Using Artificial Neural Networks in Solving Heat Conduction Problems, International Journal of Operations Research Vol. 12, No. 1, pp.016-020 , 2015.

[12] **Obed Cort´es, Gustavo Urquiza, Marco A. Cruz J. Alfredo Hern´andez**, Artificial Neural Networks for Inverse Heat Transfer Problems, Electronics, Robotics and Automotive Mechanics, 2007.

[13] **Sharath Kumar, Harsha Kumar, N. Gnanasekaran**, A NEURAL NETWORK BASED METHOD FOR ESTIMATION OF HEAT GENERATION FROM A TEFLON CYLINDER, Frontiers in Heat and Mass Transfer (FHMT), 7, 15, 2016.

[14] **S. Ghosh, D.K. Pratihar, B. Maiti and P.K. Das**, Inverse estimation of location of internal heat source in conduction, Inverse Problems in Science and Engineering, Taylor & Francis , 2011.

[15] **Yukio Hiranaka and Toshihiro Taketa**, DESIGNING, BACKWARD RANGE SIMULATOR FOR SYSTEM DIAGNOSES, Proc. XX IMEKO World Congress, 2012.

[16] **Yukio Hiranaka, Shinichi Miura, Toshihiro Taketa**, Hybrid backward simulator for determining causal heater state with resolution improvement of measured temperature

data through model conformation, ACTA IMEKO, Vol 6, No 1, pp.13-19, 2017.

[17] **Yukio Hiranaka, Shinichi Miura and Toshihiro Taketa**, Generic Causal Determination of thermal model and heat input by using backward simulator, Proc. XXII IMEKO World Congress, OR-134, 2018.9.6.

[18] **Node-RED**, https://nodered.org/